 doi:10.20944/preprints202207.0021.v1

Article

Progress in Developing a Neuromorphic Device that is Predicted to Enhance Cortical Prosthetic Vision by Enabling the Formation of Multiple Visual Geometries

Raymond Pavloski [1]

[1] Inner Psychophysics IP LLC, 330 Debbie Drive, Indiana, PA 15701, U.S.; info@innerpsychophysicsip.com
* Correspondence: rpavloski@gmail.com

Abstract: Sense element engagement theory explains how neural networks produce cortical prosthetic vision. A major prediction of the theory can be tested by developing a device which is expected to enable perception of continuous forms in altered visual geometries. The research reported here completes several essential steps in developing this device: (1) replication of simulations that are consistent with the theory using the NEST simulator, which can also be used for full-scale network emulation by a neuromorphic computer; (2) testing whether results consistent with the theory survive increasing the scale and duration of simulations; (3) establishing a method that uses numbers of spikes produced by network neurons to report the number of phosphenes produced by cortical stimulation; and (4) simulating essential functions of the prosthetic device. NEST simulations replicated early results and increasing their scale and duration produced results consistent with the theory. A decision function created using multinomial logistic regression correctly classified the expected number of phosphenes for 2080 spike number distributions for each of three sets of data, half of which arise from simulations expected to yield continuous visual forms on an altered visual geometry. A process for modulating electrical stimulation amplitude based on intermittent population recordings that is predicted to produce continuous visual forms was successfully simulated. The classification function developed using logistic regression will be used to tune this process as the scale of simulations is further increased.

Keywords: artificial neural networks; biological neural networks; cortical prosthetic vision; machine vision; neuromorphic hardware; neuroprosthesis

1. Introduction

The sense element engagement (SEE) theory of cortical prosthetic vision (CPV) was devised in order to provide a testable explanation of how neural interactions give rise to specific qualities of experience [1,2]. The phenomena of CPV were specifically chosen for explanation because the qualities of cortical prosthetic visual experience are readily amenable to mathematical modeling, elements of the resulting models can be related to models of neuron and neural network activity in a natural way, and knowledge of such relationships could lead to improvements in CPV.

1.1. The Visual Geometry and Lightness Interval Distribution of CPV

In CPV, video images captured by a camera mounted in eyeglasses control delivery of electric current that stimulates neurons in primary visual cortex (V1) [3-6]. Above-threshold current delivered through a single electrode produces the experience of a typically achromatic bright spot called a phosphene, and simultaneous delivery of current through multiple electrodes produces multiple distinct phosphenes [7-14]. Phosphenes are described as existing in the environment, and the locations of phosphenes relative to the direction of gaze are determined by placement of electrodes on V1 [7,15]. A recent investigation reported that sequentially stimulating electrodes along a path describing a

Preprints (www.preprints.org) | NOT PEER-REVIEWED | Posted: 1 July 2022 doi:10.20944/preprints202207.0021.v1

visual form led to reported experiences of that form rather than of discrete phosphenes, and it was suggested that this technique, called current steering, may produce this effect by activating visual motion circuits [9].

The size of a phosphene grows up to a saturation point with the magnitude of stimulating current [16] as well with its visual eccentricity [7,17]. The latter effect is expected from the V1 magnification factor [13], which describes how the size of the retinal region represented by neurons in a column of V1 grows with distance from the cortical representation of the fovea and therefore with visual eccentricity. The effect of magnification in CPV is apparent in Figure 1(a) which depicts a simulation of discrete phosphenes based on data reported in [16]. When this graphic is appropriately sized and the fixation point (+) is viewed from a distance of 54 cm, the visual experience should approximate the perception of four stimulation-induced phosphenes centered $(-7.5°, 8.5°)$ from the direction of gaze.

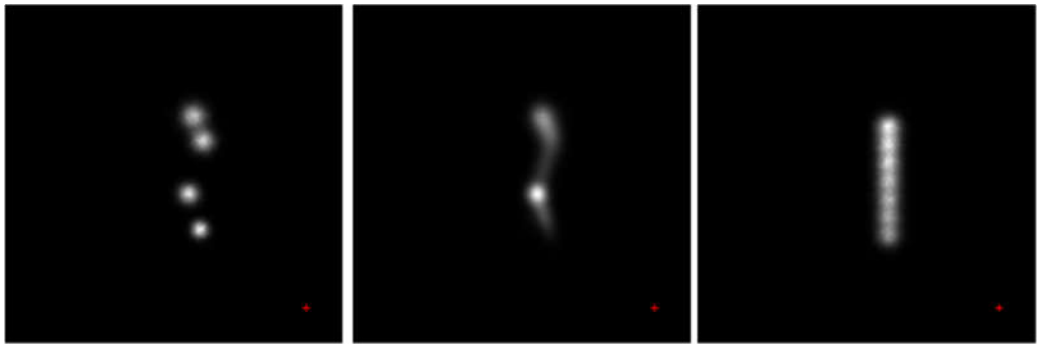

(a) **(b)** **(c)**

Figure 1. Simulations of: (**a**) four discrete phosphenes representing a vertical line; (**b**) fusion of the four phosphenes as might occur when current steering is applied or when a second visual geometry is generated using a prosthetic device as predicted by SEE theory; (**c**) an approximation to a vertical line that is predicted to result from a different alternative geometry as predicted by SEE theory.

The visual space that phosphenes inhabit can be modeled as a visual geometry [1,2] using relations between idealized, flattened V1 coordinates (x, y) and retinal eccentricity ε_r and azimuth a_r coordinates (e.g., [18] and [19], Ch. 2),

$$x = \gamma \ \ln(1 + \varepsilon_r/\varepsilon_0), \qquad y = -\gamma \ \varepsilon_r \ \pi \ a_r/(\varepsilon_0 + \varepsilon_r)180^\circ \tag{1}$$

and then approximating visual geometry coordinates $\hat{\varepsilon}$ and $\hat{a}$ by finding the inverse of equations (1),

$$\hat{\varepsilon} = \varepsilon_0[exp(x/\gamma) - 1], \tag{2}$$

$$\hat{a} = -180^\circ y \ exp(x/\gamma)/\gamma\pi[exp(x/\gamma) - 1].$$

Hats are used to decorate quantities that describe aspects of visual experience in order to distinguish them from objectively measurable quantities that describe aspects of neural networks, such as variables on which synaptic strengths depend. Values $\gamma = 12\ mm$ and $\varepsilon_0 = 1^\circ$ have been estimated from the macaque monkey [18] and are used in simulations.

An idealized flattened V1 geometry and a corresponding visual geometry created using equations (1) and (2) are depicted in Figure 2. The V1 geometry is composed of 939 idealized columns and the visual geometry of 939 corresponding visual regions. As in [1] and [2], the visual geometry was constructed by using equations (2) to transform coordinates of the center of V1 column i to values $(\hat{\varepsilon}_i, \hat{a}_i)$ of idealized visual geometry coordinates, assigning the value $(0.15 + 0.09\ \hat{\varepsilon}_i)^{1.2}$ to the radius of visual geometric region $\hat{R}_i$, and then converting $(\hat{\varepsilon}_i, \hat{a}_i)$ values to cartesian coordinates $(\hat{x}_i^\circ, \hat{y}_i^\circ)$ that specify the center

Preprints (www.preprints.org) | NOT PEER-REVIEWED | Posted: 1 July 2022 doi:10.20944/preprints202207.0021.v1

of each visual region in degrees of visual angle. It has been estimated that currents greater than 100 μA delivered through a microelectrode are likely to activate much of the volume of a V1 column [17], and the size of phosphenes that are generated using surface electrode stimulation strongly suggest that neurons in one or more columns are activated [16]. It is therefore assumed that each phosphene inhabits at least one visual geometric region $\hat{R}_i$.

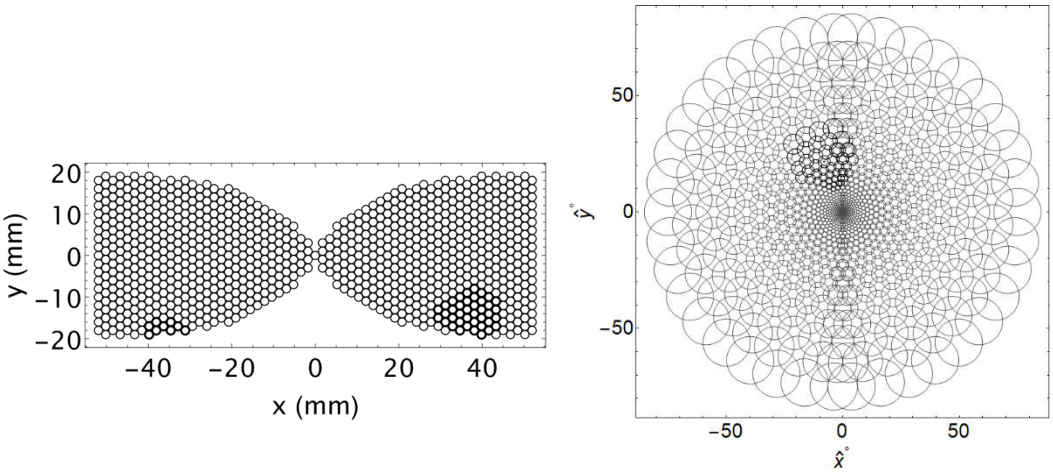

(a) **(b)**

Figure 2. An idealized V1 geometry consisting of 939 columns in which negative values of x are used for the left hemisphere is shown in panel (a) and a corresponding idealized visual geometry consisting of 939 visual regions in which negative values of $\hat{x}^\circ$denote the left visual field is shown in (b). The darker columns and regions are employed in computer simulations.

Because it seems unlikely that the lightness of a phosphene can be modeled using a real number, an interval of values is used [1,2]. It is assumed that Blue-Yellow and Red-Green opponents are activated approximately equally by electrical stimulation, thereby resulting in typically achromatic phosphenes [7,20]. Idealized lightness values are modeled by a time-dependent lightness distribution

$$\hat{l}(\hat{x}_i^\circ, \hat{y}_i^\circ, t) = s_0 f_L(x_i, y_i, t)^{l_0}. \quad (3)$$

In this equation, $f_L(x_i, y_i, t)$ is the frequency of spikes generated by a lightness channel neuron in V1 column i with center coordinates (x_i, y_i) at time t. A lightness interval distribution is mapped from the spike frequencies of a set of lightness channel neurons in each column.

1.2. Overview of SEE Theory

SEE theory is based on a perspective from which both objective and subjective aspects of the visual geometry are viewed as constituting a single pattern that arises from one system of synaptic interactions, and both aspects of the lightness interval distribution are viewed as a pattern that arises from a second system of interactions. This perspective accounts for the existence of aspects of experience as natural phenomena by assuming that the physical world provides the conditions which make the phenomena of subjective experience possible as it provides conditions that make spatial and temporal phenomena possible [21-23]. Using this assumption, SEE theory asserts that synaptic interactions occur in space (S), time (T) and sense (X) backgrounds which make possible the spatial, temporal, and sensible aspects of CPV. The visual geometry is presumed to result from interactions mediated by a geometric (G) system of synapses with strengths that are mathematical functions of distances in the visual geometry, and the lightness interval distribution is taken to result from interactions mediated by a lightness (L) system of synapses with strengths that are functions of absolute differences in lightness. The quantities ε_0 and γ in equation (2) are viewed as order parameters that characterize the SXT visual

Preprints (www.preprints.org) | NOT PEER-REVIEWED | Posted: 1 July 2022 doi:10.20944/preprints202207.0021.v1

geometry pattern, and s_0 and l_0 in equation (3) are viewed as order parameters that characterize the SXT lightness interval distribution pattern [24,25]. In particular, the visual geometry vanishes as $\varepsilon_0 \to 0$, the lightness interval distribution vanishes as $s_0 \to 0$, and both $\varepsilon_0 \to 1, s_0 \to 1$ and both patterns emerge as the frequency of extrinsically-generated spikes to excitatory neurons in the V1 neural network reaches a critical value [1,2].

Visual developmental processes are viewed as responsible for the existence of quantities that vary with visual distances and absolute differences in lightness and which underlie the strengths of G system and L system synaptic interactions between neurons that comprise a V1 network. As the frequency of extrinsic spikes which have an excitatory effect on excitatory network neurons increases, a critical value is reached at which neurons in every column of the network are active. The visual geometry and lightness interval distribution then emerge. In the language of the self-organization of patterns, the frequency of extrinsic spikes is called a control parameter [24,25]. Emergence of the visual geometry occurs as G system synaptic interactions at particular spatial locations and during specific durations of time engage collections of sets of geometric vectors. A given synaptic interaction engages a set of vectors of the same magnitude that begin in a visual region that is engaged by the presynaptic neuron and terminate in a region that is engaged by the postsynaptic neuron. The vectors relate each point in the presynaptic (postsynaptic) region to at least one point in the postsynaptic (presynaptic) region. Similarly, emergence of the lightness interval distribution occurs as L system synaptic interactions at particular spatial locations and during specific durations of time engage collections of sets of absolute differences in lightness. A specific interaction engages a set of absolute differences of the same magnitude between the lightness interval that is engaged by the presynaptic neuron and the lightness interval that is engaged by the postsynaptic neuron. The sets of absolute differences in lightness relate each lightness value in the presynaptic (postsynaptic) interval to at least one value in the postsynaptic (presynaptic) interval.

Small-scale computer simulations of neurons in 25 of the columns represented by darker circles in Figure 2a have shown that the proportion of active excitatory neurons increases rapidly with the frequency of extrinsic spikes which have an excitatory effect on excitatory network neurons, and that excitatory neurons in all regions become continuously active when the frequency is above 60 spikes/s [1,2]. This occurs both in the presence and absence of simulated stimulation and is consistent with the contention that this frequency is a control parameter with a critical value of approximately 60 spikes/s. The 25 visual regions that correspond to these columns are numbered 1-25 in Figure 3.

It was suggested that although there are several strategies that could be followed in testing SEE theory, one strategy should be given priority because of its potential benefits [1,2]. The goal of this strategy is the construction of a neuromorphic device that could be used to create a second visual geometry and thereby to produce continuous visual forms. As indicated above, the experience of unified forms has been reported to result from current steering and has been attributed to the activation of visual motion circuits [9]. According to SEE theory, appropriate modulation of G system synaptic strengths can alter shapes and sizes of regions in the visual geometry and thereby produce the experience of continuous visual forms. It was therefore hypothesized that current steering activates visual motion circuits which in turn modulate G system synaptic strengths [1,2]. If this is correct, then introducing additional interactions between populations of network neurons mediated by intermittent recording and stimulation and by neuromorphic G system synapses of appropriate strengths should create a second visual geometry that produces perception of a continuous visual form. Furthermore, it should be possible to introduce different visual forms by using different sets of neuromorphic G system synapses. Figure 1(b) is a simulation of a continuous form that is predicted to result from use of a set of neuromorphic synaptic strengths that are mapped from distances between regions corresponding to cortical columns. Figure 1(c) is a simulation of a visual form that is predicted to result from the use of neuromorphic synaptic strengths that are mapped from a rectangular organization of regions. It should be noted that formation of an alternative visual geometry is based on stimulation of each population of neurons for which there is an available electrode and

Preprints (www.preprints.org) | NOT PEER-REVIEWED | Posted: 1 July 2022 doi:10.20944/preprints202207.0021.v1

that stimulation current above the threshold for producing a phosphene is delivered through only one or a few electrodes. Additional details are provided in [1,2].

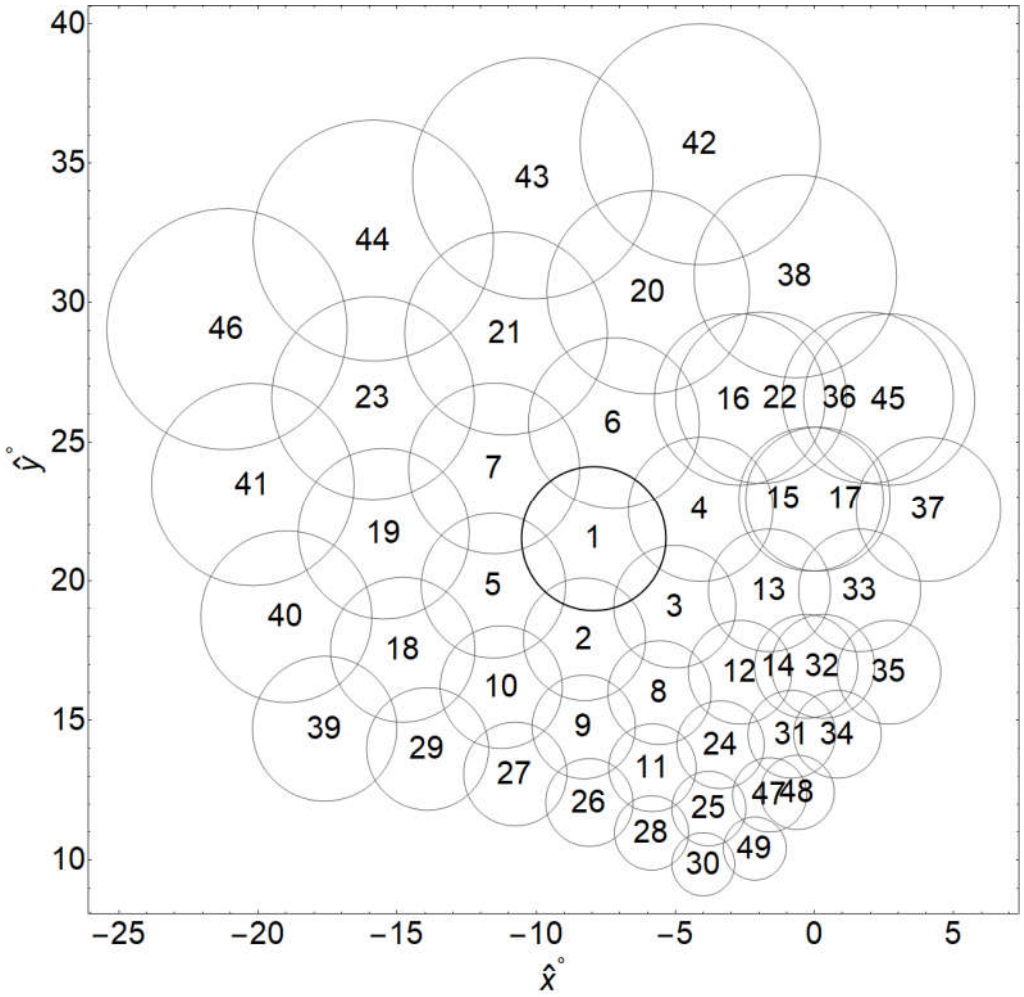

Figure 3. Visual regions corresponding to columns containing neurons that are used in computer simulations are shown using a numbering convention that is described in section 4.1. Small-scale simulations of a network consisting of neurons in columns corresponding to regions 1-25 are reported in [1,2] and are replicated here. Additional research reported in the present paper is based on simulations of neurons in columns corresponding to all 49 regions that are depicted here.

It was proposed [1,2] that emulation of a neural network that produces a full visual geometry followed by emulation of a prosthetic device that mediates the extrinsic interactions predicted to produce continuous visual forms using a neuromorphic hardware system would produce information that would be very helpful in designing a neuromorphic device that is predicted to enhance CPV. It was also proposed that these emulations should be preceded by computer simulations of increasingly larger scale that would provide values of parameters required for the emulations. The BrainScaleS computer [26] has been identified as a neuromorphic hardware system that can be used for emulation of the neural network and prosthetic device. This system uses the PyNEST interface [27] to the NEST software [28], and it was therefore decided that PyNEST and NEST should be employed for the required computer simulations.

1.3. Aims of the Present Research

The research that is reported here had the purpose of completing the following steps in development of the prosthetic device. The first step is using the PyNEST interface and the NEST simulator [27,28] to replicate the simulations of neurons in columns that correspond to visual regions numbered 1-25 in Figure 3 and reported in [1,2]. While differences

 doi:10.20944/preprints202207.0021.v1

in details of the models that are employed in the original simulation code and those employed by NEST are likely to produce some quantitative differences in results, it is crucial that NEST simulations produce results that are consistent with the theory and that they remain so as the duration of simulations is increased. The second step is determining if results consistent with the theory are obtained as the size of the network is scaled up and simulation duration is increased.

The third step addresses both conceptual and practical issues in development of the prosthetic device. As noted in [1,2], consistency demands that the perspective on which SEE theory is based should include the experience of the number of phosphenes. In particular, output of the V1 network should result in interactions beyond V1 that generate *SXT* patterns which include subjective awareness of the number of phosphenes and objective neural activity that is required to report that number behaviorally. The identification of a method that uses spikes produced by simulations of the V1 network neurons to report the number of phosphenes produced by simulated cortical stimulation would lend credence to the claim that this can be done by networks that receive input from the V1 network. Such a method would also be very useful in tuning parameters of the prosthetic device as the scale of simulations is increased. An attempt was therefore made to identify and test such a method.

Finally, the fourth step consists of simulating essential features of the sought-after device. The process that underlies the extrinsically-mediated construction of an alternative visual geometry requires cycling through intermittent population recording and stimulation, creating artificial neuron spikes from the population recordings, and using the membrane potential of a model neuron with G system conductance-based synapses that receive the spikes to modulate the amplitude of electrical stimulation to neurons in each population. PyNEST code was therefore developed in order to simulate these requirements of a device that is predicted to enable perception of continuous visual forms on an altered visual geometry.

2. Results

2.1. Replication and Increase in Duration of Neural Network Simulations Spanning 25 Cortical Columns Using NEST

A major purpose of the simulations reported in [1,2] was to determine if the frequency of extrinsically-generated excitatory action potentials was characterized by a critical value at which excitatory or inhibitory neurons in all columns were actively interacting, thereby fulfilling a necessary condition for the emergence of the expected visual geometry and lightness interval distribution patterns. Results of simulations of 1s duration showed that excitatory neurons fulfilled this condition when the putative control parameter had a value greater than 60 spikes/s, both in the absence and in the presence of simulated stimulation of neurons in the cortical column corresponding to visual region 1.

Figure 4(a) illustrates results for each second of a set of 10s NEST simulations in the absence of stimulation and Figure 4(b) provides the same results in the presence of simulated stimulation of column 1 neurons. The overall shapes of these graphs are similar to those reported in [1,2]. The most notable difference is the onset of active interactions among the neurons in all columns for lower values of the putative control parameter in the NEST simulations.

The availability of data for 10 segments of a 10s simulation illustrates temporal variability in the percentage of time that neurons in all columns are active just prior to a jump from 0% to 100%. This behavior is characteristic of the self-organization of patterns and occurs near critical values of a control parameter where changes in the value of an order parameter occur [25,26].

Preprints (www.preprints.org) | NOT PEER-REVIEWED | Posted: 1 July 2022 doi:10.20944/preprints202207.0021.v1

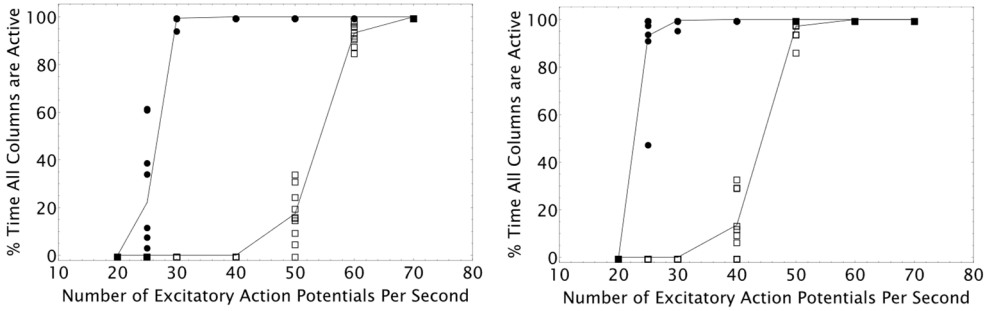

Figure 4. The percentage of the final 900 *ms* of each of 10, 1*s* segments of 10*s* simulations during which excitatory (closed disks) and inhibitory (open squares) neurons in all 25 columns are producing non-zero values in synaptic conductance in target neurons. Lines join values averaged over the 10, 1*s* intervals. Panel (a) depicts data in the absence of simulated stimulation and panel (b) shows data in the presence of simulated stimulation of column 1 neurons.

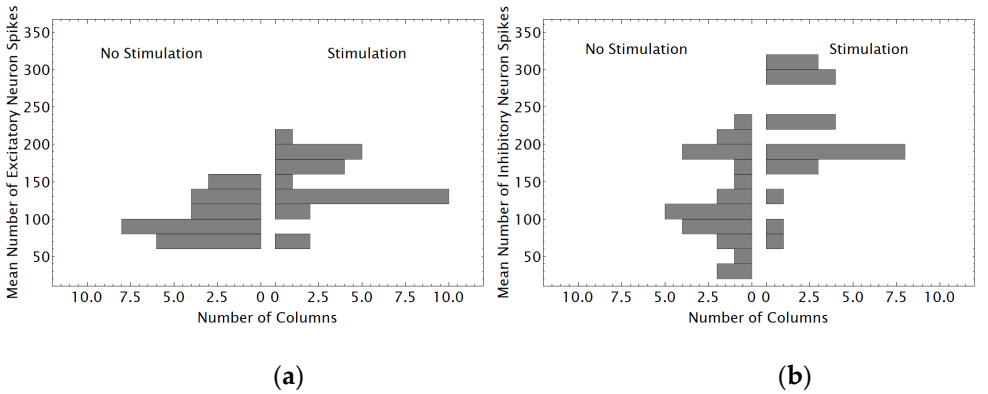

Figure 5. The distributions of numbers of spikes for network excitatory (a) and inhibitory (b) neurons in columns 1-25 averaged over 10*s* simulations are shown for both no stimulation and stimulation conditions. The frequency of extrinsic excitatory action potentials was set to 70/*s*.

Distributions of numbers of spikes produced by excitatory and inhibitory neurons obtained from the initial simulations were reported for a control parameter value of 90 spikes/*s* [1,2]. The excitatory neuron distributions for both no stimulation and stimulation conditions had a much narrower range than the inhibitory neuron distributions. Because of the lower values of the control parameter required to achieve active interactions among neurons in all columns found with NEST simulations, distributions were found using a control parameter value of 70 spikes/*s* and are displayed in Figure 5. The differences between no stimulation and stimulation conditions and between excitatory and inhibitory neurons are similar to those found in the initial simulations.

2.2. Simulations of a Neural Network Spanning 49 Cortical Columns Using NEST

Results found using 10*s* simulations of neurons in the 49 columns corresponding to the visual regions shown in Figure 3 are displayed in Figures 6 and 7. Comparison of these results with Figures 4 and 5 show that nearly doubling the scale of the simulations produces qualitatively similar results with a lower critical value of the control parameter and greater maximum values of spike numbers.

Preprints (www.preprints.org) | NOT PEER-REVIEWED | Posted: 1 July 2022 doi:10.20944/preprints202207.0021.v1

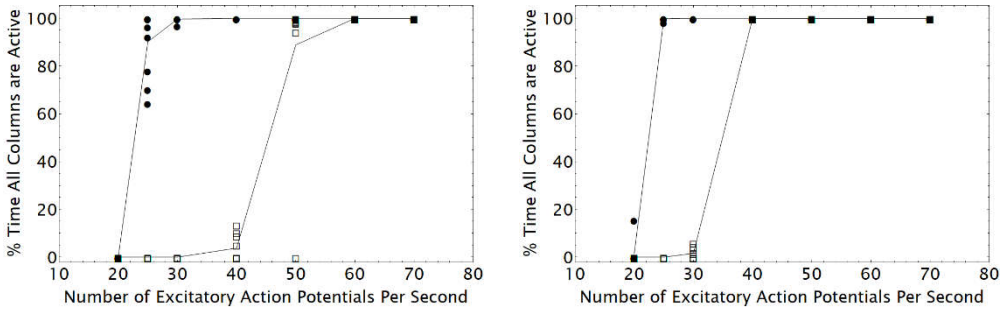

Figure 6. The results reported in Figure 4 for simulations of neurons in 25 columns are shown here for simulations of neurons in 49 columns. Although the general shapes of the average values joined by lines are similar to those found for 25 columns, the onset of continuously active neurons in all columns occurs for lower values of the control parameter.

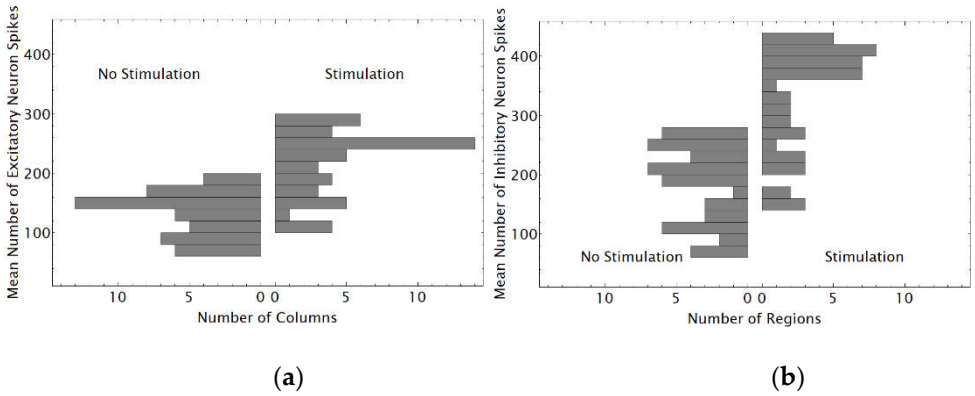

Figure 7. The distributions of numbers of spikes for network excitatory (a) and inhibitory (b) neurons in columns 1-49 averaged over 10*s* simulations are shown for both no stimulation and stimulation conditions. The frequency of extrinsic excitatory action potentials was set to 70/ *s*.

2.3. Using Distributions of Numbers of Spikes Produced by Neural Network Neurons to Detect the Number of Phosphenes

Multinomial logistic regression was used to determine if this popular and easily implemented machine learning technique could provide an accurate classification of the expected number of phosphenes using distributions of the numbers of spikes produced in 1*s* intervals of simulations of 10 *s* duration by pairs of excitatory and inhibitory neurons in all 49 columns as predictor variables. The number of spikes produced by a specific excitatory neuron and the number of spikes produced by a specific inhibitory neuron in each column during a given simulation are combined to form a 98-element vector that is a "feature" employed for determining the number of phosphenes that are present during that second of the simulation. A single simulation of neurons in 49 columns then produces 98 features that can be used for classification for each specific pair of an excitatory neuron and an inhibitory neuron, and there are 8 possible pairings of the 4 excitatory and 2 inhibitory neurons. As indicated in section 4.2 and illustrated in Table 2, a total of 2080 examples consisting of vectors of numbers of spikes and a classification as "0", "1", "2", or "3" phosphenes were used to develop a classification function for simulations in which the frequency of extrinsic, excitatory spikes was 40/*s*, 50/*s*, and 60/*s*. Half of the simulations employed G system synaptic strengths for the unaltered visual geometry shown in Figure 3 and half used G system synaptic strengths for an altered visual geometry in which regions 4 and 5 were each equal to the union of regions 1, 4, and 5.

Examples of the mean number of spikes produced by the 4 excitatory neurons and 2 inhibitory neurons in each column during the first second of a 10*s* simulation for the unaltered visual geometry shown in Figure 3 during which 40 excitatory spikes/*s* were delivered to excitatory network neurons are shown in Figure 8. The cases depicted in Figure

Preprints (www.preprints.org) | NOT PEER-REVIEWED | Posted: 1 July 2022 doi:10.20944/preprints202207.0021.v1

8a were chosen because they illustrate dramatic differences in the spike distributions when no simulated stimulation is delivered (top panel) and when neurons in either column 1 (middle panel) or column 12 (bottom panel) are stimulated. The distributions shown in Figure 8b were chosen because they illustrate what appear to be cases for which correct classification of numbers of phosphenes may be much more challenging. Visual regions 1 and 4 and regions 1 and 5 overlap, and therefore the cases in which columns that correspond to regions 1 and 4, 1 and 5, and 1, 4, and 5 are stimulated are all expected to give rise to a single phosphene. However, stimulation of columns corresponding to visual regions 4 and 5, which do not overlap, is expected to give rise to two phosphenes.

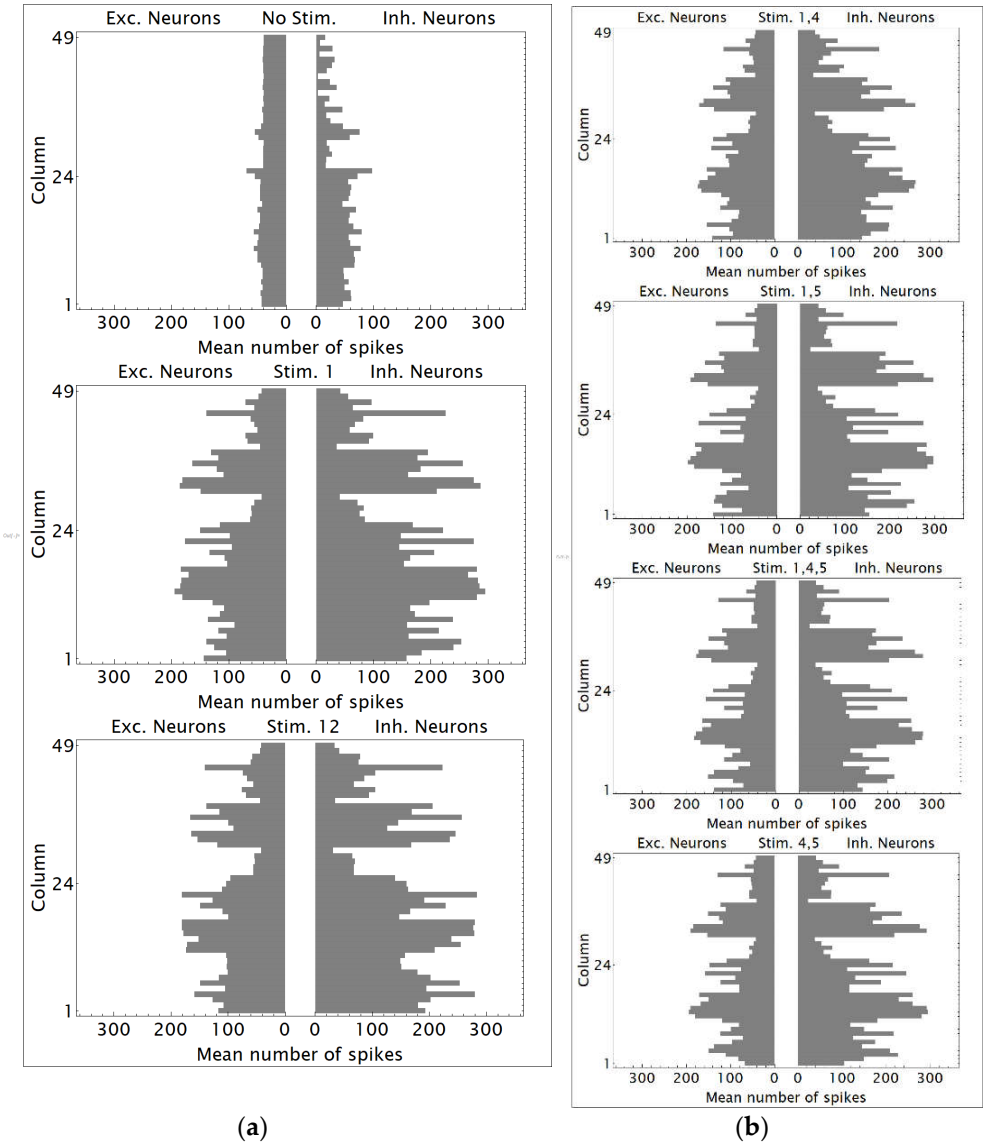

(**a**) (**b**)

Figure 8. Examples of distributions of mean numbers of spikes produced by the neurons in each column during the first second of a 10*s* simulation in which 40 excitatory spikes/*s* were delivered to excitatory network neurons. (a) There are clear differences between the distributions in (a) but those in (b) appear to be more similar and suggest that correct classification of the expected number of phosphenes would be difficult.

Preprints (www.preprints.org) | NOT PEER-REVIEWED | Posted: 1 July 2022 doi:10.20944/preprints202207.0021.v1

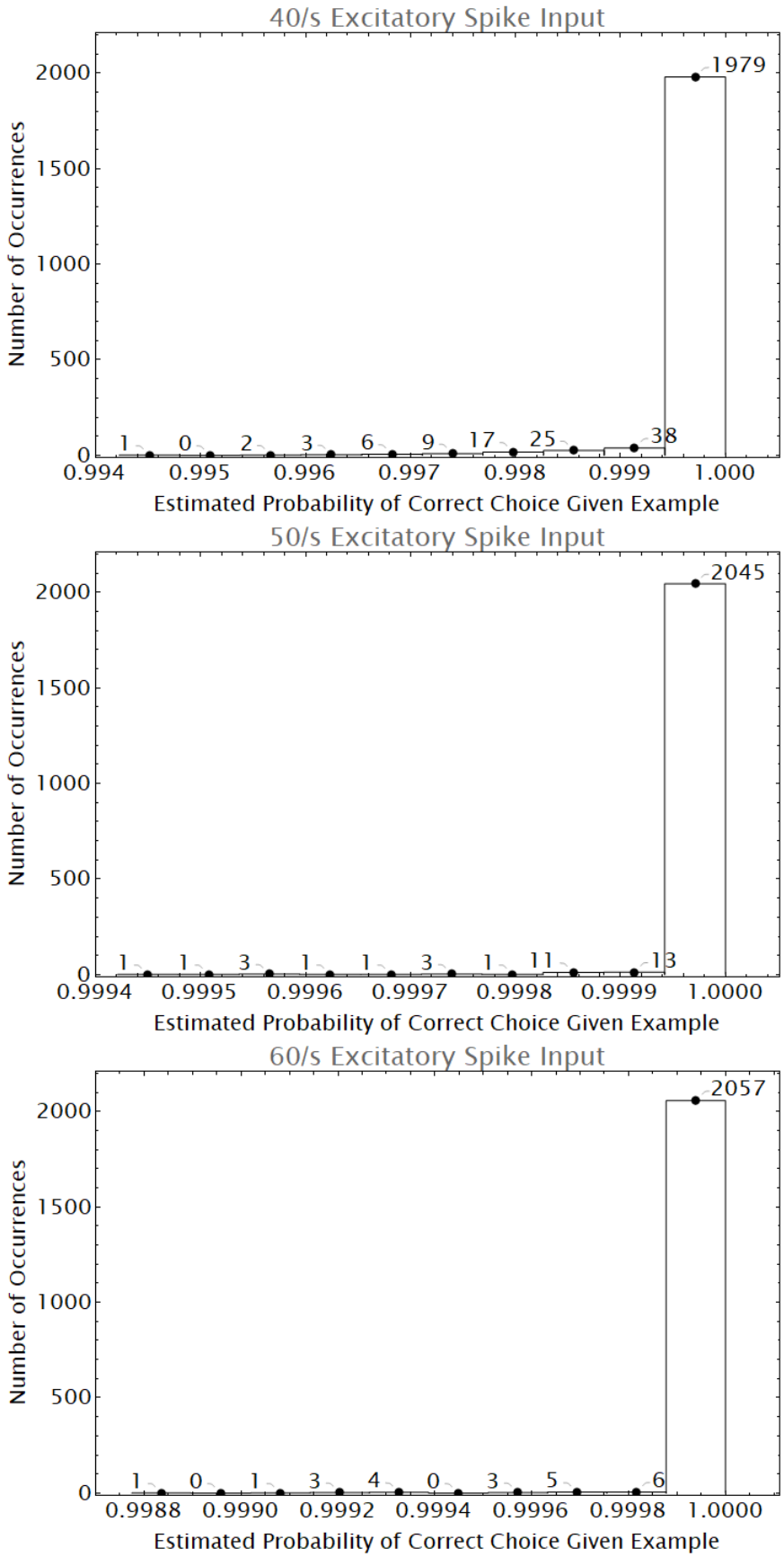

Figure 9. The frequency of occurrence of all posterior probability estimates for correct choices given each of the 2080 examples are shown for simulations in which the control parameter has values of 40/*s*, 50/*s*, and 60/*s*. Bin widths are 5.7777×10^{-4}, 5.7943×10^{-5}, and 1.2255×10^{-4} from top to bottom.

Preprints (www.preprints.org) | NOT PEER-REVIEWED | Posted: 1 July 2022 doi:10.20944/preprints202207.0021.v1

Given the apparent difficulty of the classification task, it may be surprising that each of the 2080 classifications produced by the resulting classification function was correct for excitatory spike frequencies of 40/*s*, 50/*s*, and 60/*s*. The mean cross entropy values (see section 4.2) for simulations with excitatory spike frequencies of 40/*s*, 50/*s*, and 60/*s* were 9.81×10^{-5}, 3.40×10^{-6}, and 6.81×10^{-6}, respectively. Furthermore, the multinomial logistic regression model's estimated conditional (posterior) probabilities of the correct number of phosphenes given each of the 2080 spike number examples are extremely high, as shown in Figure 9. These data show that numbers of excitatory and inhibitory spikes can be used to classify the number of phosphenes with great accuracy even when the data arise from a mixture of visual geometries.

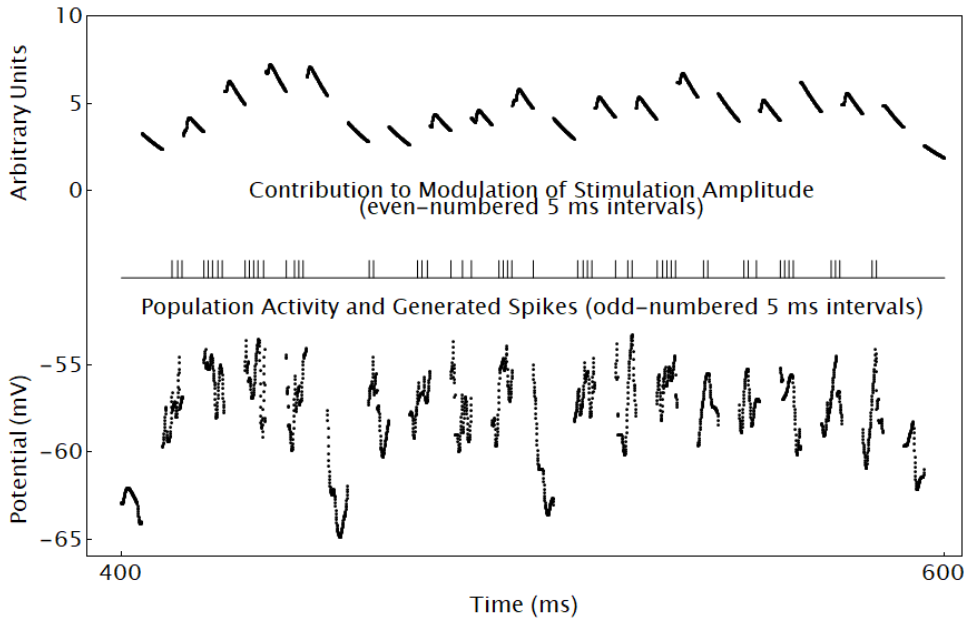

Figure 10. Simulated activity of column 1 neurons and simulated spikes resulting from values greater than -57 *mV* are shown during odd-numbered 5 *ms* intervals, and the membrane potential of a model neuron that is influenced by these spikes via G system synapses is shown during even-numbered 5 *ms* intervals. Data are displayed for 200 *ms* in order to provide a clear visualization of the data for each interval and the impact of spikes on the contribution of column 1 activity to modulation of intermittent stimulation of column 1 neurons.

2.4. Simulating Essential Features of a Prosthetic Device that is Predicted to Create a Visual Geometry

It was proposed in [1,2] that producing a second visual geometry in order to create unified visual forms requires:

1. Using electrodes to stimulate and to record activity intermittently from each population for which an electrode is available;
2. Generating a neuromorphic spike if population activity is greater than a threshold;
3. Delivering spikes from all populations to a model neuron for each population via G system conductance-based synapses; and
4. Using the membrane potential of each model neuron to determine the contribution of the recorded activity to modulation of stimulation amplitude for each population.

The essential functions of the proposed device are illustrated in Figure 10 using data from a 1*s* simulation in which neurons in columns 1 and 12 received simulated stimulation, 40 extrinsic spikes/*s* were delivered to excitatory network neurons, G system synaptic strengths were based on an unaltered visual geometry, and the membrane potential of a single model neuron was recorded. Population activity of column 1 neurons was simulated by computing the average membrane potential of the 4 excitatory and 2 inhibitory neurons during odd-numbered 5 *ms* intervals, thereby providing 100 samples for each

Preprints (www.preprints.org) | NOT PEER-REVIEWED | Posted: 1 July 2022 doi:10.20944/preprints202207.0021.v1

such interval. A spike was generated at time t^* during an odd-numbered interval if simulated population activity was greater than a threshold of $-57\ mV$ and at least 1 ms had passed since the previous spike occurred. This threshold was found to yield a number of model spikes that is sufficient to provide a visualization of their impact on a model neuron's membrane potential.

The spikes that were generated on odd-numbered 5 ms intervals were delivered to an integrate and fire model neuron with conductance-based synapses and G system strengths based on distances from visual region 1 to itself, thereby modulating the neuron's membrane potential on even-numbered 5 ms time intervals. Inspection of Figure 10 shows that fluctuations in the simulated population activity produce corresponding changes in the population's contribution to the modulation of stimulation amplitude.

3. Discussion

The research reported here is based on SEE theory, which portrays the subjective and objective aspects of CPV as jointly constituting sensible spatiotemporal patterns, and which makes possible the prediction that particular alterations in the strengths of certain G system synaptic interactions will produce a specific change in the pattern of phosphenes [1,2]. The theory moves past what were previously only suggestive relationships between activity in neural network simulations and specific aspects of visual experiences [31-34] by providing a strategy for developing a neuromorphic device that is predicted to yield perception of continuous visual forms within alternate visual geometries. The results reported here signify progress in following this strategy.

Like the initial simulations [1,2], simulations run using PyNEST demonstrated that the frequency of excitatory spikes generated outside the neural network is characterized by a critical value above which neurons in all columns actively interact, thereby fulfilling a necessary condition for self-organization of the visual geometry and lightness interval distribution patterns. Furthermore, the NEST simulations extended this finding from 25 columns of neurons to 49 columns and from a duration of 1 s to a duration of 10 s.

Multinomial logistic regression was applied to the problem of determining if distributions of numbers of spikes produced by the excitatory and inhibitory neurons that populate columns of the network can be used to determine the number of phosphenes that are produced by simulated stimulation of one or more columns. Results show that perfect classifications of phosphene numbers are found even though the data are derived from a mixture of visual geometries. These results are consistent with SEE theory's contention that networks receiving spike trains from V1 produce patterns that include subjective awareness of the number of phosphenes and objective neural activity which is used to report that number behaviorally. In addition, the results suggest that multinomial logistic regression can be used to adjust parameters of neuromorphic device simulations in efforts to alter visual geometries for which expected numbers of phosphenes are reported.

The basic and essential functions of the neuromorphic device were also simulated. It was shown that intermittent simulated stimulation of a population of neurons in each column for which an electrode is available can be modulated by the intermittently recorded electrical activity of each population in a way that is consistent with the stated requirements of the device [1,2].

These results will be employed in the following steps toward full emulation using BrainScaleS [26] hardware:

1. Extending the application of multinomial logistic regression to data obtained from simulations of multiple altered visual geometries;
2. Using the classification functions obtained from multinomial logistic regression to determine if distributions of numbers of spikes that are produced through simulations of the sought-after prosthetic device yield correct number of phosphene reports and to adjust parameters of the simulations if necessary;

Preprints (www.preprints.org) | NOT PEER-REVIEWED | Posted: 1 July 2022 doi:10.20944/preprints202207.0021.v1

3. Determining if the numbers of spikes produced by network excitatory and inhibitory neurons continue to increase with the scale of simulations and using this information to adjust coefficients of synaptic strengths if necessary (see section 4.1); and
4. Increasing the number of distances between regions and the number of absolute differences in lightness between lightness intervals on which the strengths of G system and L system synapses depend in an effort to ensure that they suffice for the formation of visual geometry and lightness interval distribution patterns.

4. Materials and Methods

4.1. Computer Simulations

Neural network simulations using NEST 2.20.0 [28] with a timestep of 0.05 ms running on Virtual Box lubuntu 18.04 followed the format of the simulations reported in [1,2], but the duration of simulations was increased from 1 s to 10 s. Spiking neurons were simulated using the simple conductance based leaky integrate-and-fire neuron model with static synapses and resting potential $-70\ mV$, membrane capacitance 250 pF, a refractory period of 2 ms for excitatory neurons and 1 ms for inhibitory neurons, threshold potential $-52\ mV$, reset potential $-59\ mV$, a rise time of the excitatory synaptic conductance alpha function equal to 0.4 ms and a rise time of the inhibitory conductance function equal to 0.2 ms. It should be noted that the NEST neuron model and the synaptic function differ from the models used in [1,2] and are expected to produce results that differ slightly from simulations that are reported in [1,2]. However, it seems reasonable to demand that the qualitative behavior of the proposed V1 network should be robust to such differences.

Four excitatory and two inhibitory neurons populated each simulated V1 column corresponding to a visual region. Simulations of networks spanning 25 columns and 49 columns were conducted. In both cases, the 7 regions having the smallest center-to-center visual distances from each of the 939 regions were found and defined as nearest neighbors (nn) of that region. The region numbered 298 with center coordinates $(-7.9358°, 21.5206°)$ was arbitrarily identified as the core region of the simulation as in [1,2] and renumbered as region 1. The 7 nn of region 1 were first identified and numbered 2-8. The 7 nn of each of regions 2-8 were then identified and numbered 9-25. In order to simulate the neurons in the corresponding columns, the 7 nn of regions 9-25 were identified but only those regions that are members of the original set of 25 were retained. In simulations of 49 regions, all 7 nn of regions 9-25 were retained and the 24 regions not contained in the original set of 25 were numbered 26-49. The 7 nn of these 24 regions were identified, but only those regions that are members of the original set of 49 were retained. The identities of all regions are provided in Table 1, with the nn of the initial set of 25 shown in boldface type.

Each excitatory neuron and each inhibitory neuron in each of the columns corresponding to the simulated regions received input from each excitatory neuron in its nn columns (including neurons in its own column other than itself) via $n_e = 7$ synapses, and from each inhibitory neuron in its nn columns (including the inhibitory neuron in its own column other than itself) via $n_i = 2$ synapses. Synaptic strengths were determined using the maximum visual distance $(d_{i,j})_M$ between regions and the maximum difference in lightness between regions $|\delta l_{i,j}|_M$ under the assumption that order parameters $\varepsilon_0 = s_0 = 1$. This procedure was chosen over the strategy used in [1,2] of allowing the order parameters to vary according to potential functions (described by equations (4), (5), (7), and (8) in [2]) in order to speed up simulations. G system synaptic strengths were assigned using

$$G_{i,j,\alpha} = \begin{cases} G_M - \dfrac{G_M}{(d_{i,j})_M} d_{i,j,\alpha}, & d_{i,j,\alpha} \le (d_{i,j})_M \\ 0, & d_{i,j,\alpha} > (d_{i,j})_M. \end{cases} \quad (4)$$

Preprints (www.preprints.org) | NOT PEER-REVIEWED | Posted: 1 July 2022 doi:10.20944/preprints202207.0021.v1

The maximum strength $G_M = 1$, the maximum distance $(d_{i,j})_M = 39.2183$ between two points in nn regions within the entire set of 939 regions, $d_{i,j}$ is a specific distance between a point in column i containing the presynaptic neuron and a point in region j containing the postsynaptic neuron, and α identifies the synapse.

Table 1. Nearest neighbors of each of the 49 regions that are shown in Figure 3. Regions in the initial set of 25 are numbered with bold typeface.

Region	Nearest Neighbors							Region	Nearest Neighbors						
1	**2**	**3**	**4**	**5**	**6**	**7**	**8**	26	28	11	9	27			
2	**9**	**8**	**10**	**3**	**1**	**5**	**11**	27	26	9	10	29			
3	**8**	**12**	**13**	**2**	**4**	**1**	**14**	28	30	25	11	26			
4	**3**	**13**	**15**	**1**	**16**	**17**	**6**	29	27	10	18	39			
5	**10**	**2**	**18**	**1**	**7**	**19**	**9**	30	49	25	28				
6	**1**	**4**	**16**	**7**	**20**	**21**	**22**	31	34	48	47	14	24	32	
7	**5**	**1**	**6**	**19**	**21**	**23**	**2**	32	14	35	34	31	12	33	13
8	**11**	**24**	**9**	**12**	**3**	**2**	**25**	33	32	35	13	14	17	15	
9	26	**11**	**8**	27	**2**	**10**	28	34	31	32	48	14			
10	27	**9**	29	**2**	**5**	**18**	26	35	32	34	14	33			
11	28	**25**	26	**24**	**8**	**9**	30	36	45	22	17	15	37	16	
12	**14**	**24**	31	32	**8**	**13**	**3**	37	33	17	45	15			
13	**14**	**12**	33	32	**3**	**15**	**17**	38	22	16	36	20	45		
14	32	**12**	31	34	35	**13**	33	38	29	18	40				
15	**17**	**13**	33	**4**	**22**	36	37	40	39	18	19	41	29		
16	**22**	**4**	**15**	**17**	36	**6**	38	41	40	19	23	46	18		
17	**15**	33	**13**	37	36	**22**	**4**	42	20	38	43				
18	29	**10**	**5**	39	**19**	40	27	43	21	20	44	42			
19	**18**	**5**	**7**	40	**23**	41	**10**	44	23	41	46	43	7		
20	**6**	**16**	38	**21**	**22**	42	43	45	36	37	17	15	22		
21	**7**	**6**	**23**	**20**	43	44	**1**	46	41	23	44	19			
22	**16**	36	**15**	**17**	38	**4**	45	47	48	49	25	31			
23	**19**	**7**	**21**	42	44	46	**5**	48	47	31	49				
24	**25**	47	31	**11**	**12**	**8**	48	49	30	47	25				
25	30	49	47	28	**24**	**11**	48								

L system synaptic strengths were found for the case in which no simulated electrical stimulation was delivered and for a number of cases in which simulated electrical stimulation was delivered to one or more regions. It was assumed that lightness system neurons in each non-stimulated column had a minimum frequency of 10 action potentials per second and a maximum frequency of 20 action potentials per second and that stimulation yielded a minimum frequency of 90 per second and a maximum frequency of 100 per second. Assignment of strengths was based on

$$L_{i,j,\beta} = \begin{cases} L_M - \dfrac{L_M}{|\delta l_{i,j}|_M}|\delta l_{i,j,\beta}|, & |\delta l_{i,j,\beta}| \le |\delta l_{i,j}|_M \\ 0, & |\delta l_{i,j,\beta}| > |\delta l_{i,j}|_M. \end{cases} \quad (5)$$

The maximum strength $L_M = 1$, $|\delta l_{i,j}|$ denotes a specific absolute difference in lightness between region i and region j, the maximum difference in lightness is given by $|\delta l_{i,j}|_M$, and β identifies the synapse. In the case of no simulated stimulation $|\delta l_{i,j}|_M = 5.42247$ and in the presence of simulated electrical stimulation $|\delta l_{i,j}|_M$ had a minimum value of 35.8929 and a maximum value of 37.3426.

Preprints (www.preprints.org) | NOT PEER-REVIEWED | Posted: 1 July 2022 doi:10.20944/preprints202207.0021.v1

Individual G system synaptic strengths were determined by choosing n_e or n_i values for distance variables $d_{i,j,\alpha}$ that are uniformly distributed in the interval $0.9\,\langle d_{i,j}\rangle < d_{i,j,\alpha} < 1.1\,\langle d_{i,j}\rangle$, in which $\langle d_{i,j}\rangle$ equals the average of the minimum and maximum distances between regions i and j. Similarly, individual L system synaptic strengths were determined by choosing n_e or n_i values for absolute differences in variables $|\delta l_{i,j,\beta}|(t)$ that are uniformly distributed in the interval $0.9\,\langle|\delta l_{i,j}|\rangle < |\delta l_{i,j,\beta}| < 1.1\,\langle|\delta l_{i,j}|\rangle$ where $\langle|\delta l_{i,j}|\rangle$ is the average of the minimum and maximum differences in lightness between the lightness intervals on regions i and j.

Simulations were also performed with an altered visual geometry in which both region 4 and region 5 were set equal to the union of regions 1, 4, and 5. In these simulations, all G system synaptic strengths to and from regions 4 and 5 were modified by finding new minimum and maximum distances within regions 4 and 5 and between regions 4 and 5 and their nearest neighbors. The minimum and maximum distances were used to find new mean distances, which were in turn used to calculate new mean G system synaptic strengths and unique strengths for each synapse.

An algorithm described in [1,2] was employed to calculate the times of simulated excitatory action potentials delivered to excitatory network neurons (i.e., the putative control parameter). Synchronous input to neurons was avoided by generating a spike train independently for each excitatory network neuron. A PyNEST script read files of these times and spike generators were employed to produce spikes. The production of times of occurrence of the desired number of additional action potentials in axons having different spatial orientations and locations from a stimulating electrode was simulated using the same algorithm. Because NEST does not provide a means for adding spike times to a running simulation, a spike generator for each neuron produced conductance changes using nearest neighbor synapses of the same strengths as those used by network neurons. Following completion of a simulation, the number of spikes produced in each second by each excitatory neuron and each inhibitory neuron in stimulated columns was increased by 95 in order to establish consistency with setting the frequency of spikes produced by lightness neurons in stimulated columns to a value between 90 and 100 spikes/s.

A coefficient having the value 2.106 multiplied the strength of each synapse from an external excitatory neuron to an excitatory network neuron, and a coefficient having the value 2.75 multiplied the strength of each synapse between a pair of network neurons. These values were selected in order to make numbers of spikes produced by neurons in small test networks similar to those produced by network neurons and reported in [1,2].

4.2. Multinomial Logistic Regression Classification of Numbers of Spikes Produced by Excitatory and Inhibitory Neurons in 49 Columns

Let $x_i^T = \left(Nexc_{i,1},\ Ninh_{i,1},\ Nexc_{i,2}, Ninh_{i,2}, \dots, Nexc_{i,N}, Ninh_{i,N}\right)$ be the i^{th} collection of pairs of numbers of spikes produced by an excitatory neuron and an inhibitory neuron in each of the $N = 49$ columns. A training data set that is to be classified consists of pairs (x_i, y_j) where each $y_j \in \{"0","1","2","3"\}$ and denotes the number of phosphenes that are present in the visual geometry. The posterior probability of class y_j given x_i is $Pr(y_j|x_i) = \exp\left(\beta_{y_j}^T \cdot x_i\right)/\sum_j^K \exp\left(\beta_{y_j}^T \cdot x_i\right)$, where the number of classes is $K = 4$ and each $\beta_{y_j}^T = (\beta_{y_{j,1}}, \beta_{y_{j,2}}, \dots, \beta_{y_{j,2N}})$ has as elements the model parameters for class y_j (other than a bias term that is omitted for brevity of notation, as noted by [29]). Denote the entire parameter set for all K classes as $\theta = \{\beta_{y_1}^T, \beta_{y_2}^T, \dots, \beta_{y_K}^T\}$ and the probability of an example x_i belonging to class y_j given θ as $p_{y_j}(x_i;\theta)$. With M collections of numbers of spike vectors in the training set, parameters are estimated by minimizing the loss function

$$\sum_{i=1}^{M} -log\left(p_{y_j}(x_i;\theta)\right) + \lambda_1 \sum_{i=1}^{n} \left|\beta_{y_{j,i}}\right| + \frac{\lambda_2}{2} \sum_{i=1}^{n} \beta_{y_{j,i}}^2. \quad (6)$$

Preprints (www.preprints.org) | NOT PEER-REVIEWED | Posted: 1 July 2022 doi:10.20944/preprints202207.0021.v1

The logistic regression function available in Mathematica was used with the default setting $\lambda_1 = 0$ and an optimization algorithm that approximates the Broyden-Fletcher-Goldfarb-Shanno algorithm using a limited amount of computer memory [30].

The numbers of spikes were obtained from simulations in which columns 1, 4, 5, or 12 might receive simulated electrical stimulation. As shown in Table 2, the stimulated columns used in simulations were none, column 1, column 4, column 5, column 12, columns 1 and 4, columns 1 and 5, columns 1, 4, and 5, columns 4 and 5, columns 1 and 12, columns 4 and 12, columns 5 and 12, and columns 4, 5, and 12. The data that were classified were obtained from simulations in which G system strengths were based on the unaltered regions depicted in Figure 3, and from simulations in which G system strengths were based on an altered visual geometry in which both regions 4 and 5 were made equal to the union of regions 1, 4, and 5. The altered visual geometry required changes in G system strengths to and from neurons in columns 4 and 5 that follow from changes in minimum and maximum visual distances (see equation 4).

Table 2. The 13 conditions that provide examples and classifications of numbers of phosphenes for the non-altered and altered visual geometry.

Expected Number of Phosphenes		Regions Stimulated
Non-Altered Visual Geometry	Altered Visual Geometry	
0	0	None
1	1	1
1	1	4
1	1	5
1	1	12
1	1	1,4
1	1	1,5
1	1	1,4,5
2	1	4,5
2	2	1,12
2	2	4,12
2	2	5,12
3	2	4,5,12

Training set spike times were obtained for each second of each simulation. For e_j examples of spike number vectors classified as y_j, the total number of examples used to find the best-fit model is $2080 = 2 \times 10 \times (N_E \times N_I) \times \sum_{j=1}^{4} e_j$ in which both unaltered and altered visual geometry simulations are used, there are 10, 1-second intervals available, $N_E = 4$ and $N_I = 2$ denote the number of excitatory and inhibitory neurons per region, and $\sum_{j=1}^{4} e_j = 13$ for the 4 possible number-of-phosphene classifications.

5. Patents

A provisional patent application for the sense element engagement process has been submitted [1]. A second provisional patent application for the material provided in this paper has been submitted [35].

Supplementary Materials: Computer code that can be used to replicate the simulations reported in this paper are provided in Python written for the PyNEST interface to NEST version 2.20.0 Virtual Box lubuntu 18.04. Code that was developed to generate parameter values and certain spike times to be used in the NEST simulations and to analyze data created by NEST simulations are provided in Mathematica version 12.2.0.0 as text files. All software is © 2022 Raymond Pavloski, PhD.

Funding: This research received no external funding.

Data Availability Statement: Simulation data that provided the results reported in this paper are protected by U.S. Provisional Patent Application Nos. 63/287,286 and 63/354,959. Please contact the author if you wish to access these data.

Conflicts of Interest: The author has submitted a provisional patent application [1] for the sense element engagement process and a second provisional patent application for the material reported in this paper [35].

References

1. Pavloski, R. Sense Element Engagement Theory Explains How Neural Networks Produce Cortical Prosthetic Vision. U.S. Provisional Patent Application No. 63/287,286, December 8, 2021.
2. Pavloski, R. Sense element engagement theory explains how neural networks produce cortical prosthetic vision. *IEEE Trans. Neural Netw. Learn. Syst.*, **2021**, *Submitted*. Preprint available online: https://www.techrxiv.org/articles/preprint/Sense_Element_Engagement_Theory_Explains_How_Neural_Networks_Produce_Cortical_Prosthetic_Vision/17161187/1
3. Gutierrez, G. Orion shines a light in the dark for the blind, Baylor College of Medicine Blog, July, 2019. Available online: https://blogs.bcm.edu/2019/07/11/from-the-labs-orion-turns-on-a-light-in-the-dark-for-the-blind/
4. Fernández, E.; Normann, R.A. CORTIVIS approach for an intracortical visual prosthesis. In *Artificial Vision: A Clinical Guide*; Gabel, V.P., Ed.; Springer: Munich, D.E. 2017; pp. 191-201.
5. Lowery, A.J.; Rosenfeld, J.V.; Rosa, M.G.P.; Brunton, E.; Rajan, R.; Mann, C.; Armstrong, M.; Mohan, A.; Josh, H.; Kleeman, L.; Li, W.H.; Pritchard, J. Monash vision group's Gennaris cortical implant for vision restoration. In *Artificial Vision: A Clinical Guide*; Gabel, V.P. Ed.; Springer: Munich, D.E. 2017; pp. 215-225.
6. Troyk, P.R. The intracortical visual prosthesis project. In *Artificial Vision: A Clinical Guide;* Gabel, V.P. Ed.; Springer: Munich, D.E. 2017; pp. 203-214.
7. Bosking, W.H.; Beauchamp, M.S.; Yoshor, D. Electrical stimulation of visual cortex: Relevance for the development of visual cortical prosthetics, *Ann. Rev. Vision Sci*., **2017**, *3*, 141-166. DOI: 10.1146/annurev-vision-111815-114525
8. Bak, M.I.; Girvin, J.P.; Hambrecht, F.T.; Kufta, C.V.; Loeb, G.E.; Schmidt, E.M. Visual sensations produced by intracortical microstimulation of the human occipital cortex, *Med. & Biol. Eng. & Comp.*, **1990**, *28*, 257-259. DOI: 10.1007/BF02442682
9. Beauchamp, M.S.; Oswalt, D.; Sun, P.; Foster, B.L.; Magnotti, J.F.; Niketeghad, S.; Pouratian, N.; Bosking, W.H.; Yoshor, D. Dynamic stimulation of visual cortex produces form vision in sighted and blind humans, *Cell*, **2020**, *181*, 774-783. DOI: https://doi.org/10.1016/j.cell.2020.04.033
10. Brindley, G.S.; Lewin, W.S. The sensations produced by electrical stimulation of the visual cortex. *J. of Physiology*, **1968**, *196*, 479-493. DOI: https://doi.org/10.1113/jphysiol.1968.sp008519
11. Doebelle, W.H. Artificial vision for the blind by connecting a television camera to the visual cortex. *Amer. Soc. of Artificial Internal Organs J.*, **2000**, *46*, 3-9.
12. Doebelle, W.H.; Quest, D.O.; Antunes, J.L.; Roberts, T.S.; Girvin, J.P. Artificial vision for the blind by electrical stimulation of the visual cortex, *Neurosurgery*, **1979**, *5*, 521-527. DOI: https://doi.org/10.1227/00006123-197910000-00022
13. Schiller, P.H.; Tehovnik, E.J. Visual prosthesis. *Perception*, **2008**, *37*, 1529-1559. DOI: 10.1068/p6100
14. Schmidt, E.M.; Bak, M.J.; Hambrecht, F.T.; Kufta, C.V.; O'Rourke, D.K.; Vallabhanath, P. Feasibility of a visual prosthesis for the blind based on intracortical microstimulation of the visual cortex. *Brain*, **1996**, *119*, 507–522. DOI: 10.1093/brain/119.2.507
15. Rushton, D.N.; Brindley, G.S. Short- and long-term stability of cortical electrical phosphenes. In *Physiological Aspects of Clinical Neurology;* Rose, R.C. Ed.; Blackwell Scientific Publishing: London, UK: 1997, pp. 123-153.
16. Bosking, W.H.; Sun, P.; Ozker, M.; Pei, X.; Foster, B.L.; Beauchamp, M.S.; Yoshor, D. Saturation in phosphene size with increasing current levels delivered to human visual cortex. *J. Neurosci.*, **2017**, *37*, 7188-7197. DOI: https://doi.org/10.1523/JNEUROSCI.2896-16.2017
17. Tehovkik, E.J.; Slocum, W. M. Phosphene induction by microstimulation of macaque V1. *Brain Res. Rev.*, **2007**, *53*, 337-343. DOI: https://doi.org/10.1016/j.brainresrev.2006.11.001
18. Tootell, R.B.; Silverman, M.S.; Switkes, E.; DeValois, R.L. Deoxyglucose analysis of retinotopic organization in primate striate cortex. *Science*, **1982**, *218*, 902-904. DOI: https://www.science.org/doi/10.1126/science.7134981
19. Dayan, P.; Abbott, L.F. Theoretical Neuroscience: Computational and Mathematical Modeling of Neural Systems. The MIT Press: Cambridge, MA, USA, 2001.
20. Lewis, P.M.; Rosenfeld, J. V. Electrical stimulation of the brain and the development of cortical visual prostheses: An historical perspective. *Brain Res.*, **2016**, *1630*, 208-224. DOI: https://doi.org/10.1016/j.brainres.2015.08.038
21. Eddington, A.S. *The nature of the physical world*. The Macmillan Company: New York, NY, USA, 1928. Available: https://openlibrary.org/books/OL15026629M/The_nature_of_the_physical_world#:~:text=Subjects%20%20%20%20Edition%20%20%20,cccc%20Borrow%20Listen%20Download%20for%20print-di%20...%20
22. Hut, P.; Shepard, R.N. Turning 'the hard problem' upside down & sideways. *J. Consciousness Studies*, **1996**, *3*, 313-329.

23. Hut, P.; Goodwin, B.; Kauffman, S. Complexity and functionality: A search for the Where, the When, and the How. *Proc. of the Int. Conf. on Complex Syst.*, Nashua, NH, USA, Sept. 21-26, 1997. Available: Complexity_and_Functionality_A_Search_for_the_Wher.pdf
24. Schöner, G.; Kelso, J.A.S. Dynamic pattern generation in behavioral and neural systems. *Science*, **1988**, *239*, 1513-1520. Available: https://www.jstor.org/stable/1701854
25. Kelso, J.A.S. Dynamic patterns: The self-organization of brain and behavior, The MIT Press: Cambridge, MA, USA, 1995.
26. Pehle, C.; Billaudelle, S.; Cramer, B.; Kaiser, J.; Schreiber, K.; Stradmann, Y.; Weis, J.; Leibfried, A.; Müller, E.; Schemmel, J. The BrainScaleS-2 accelerated neuromorphic system with hybrid plasticity. *Frontiers in Neuroscience,* **2022**, *16*, DOI: 10.3389/fnins.2022.795876
27. Eppler, J.M.; Helias, M.; Muller, E.; Diesmann, M.; Gewaltig, M-O. PyNEST: A convenient interface to the NEST simulator. *Frontiers in Neuroinformatics, 2*, **2008**, DOI: 10.3389/neuro.11.012.2008
28. Fardet, T.; Vennemo, S.B.; Mitchell, J.; Mørk, H.; Graber, S.; Hahne, J.; Spreizer, S.; Deepu, R.; Trensch, G.; Weidel, P.; Jordan, J.; Eppler, J.M.; Terhorst, D.; Morrison, A.; Linssen, C.; Antonietti, A.; Dai, K.; Serenko, A.; Cai, B.; Kubaj, P.; Gutzen, R.; Jiang, H.; Kitayama, I.; Jürgens, B.; Plesser, H.E. NEST 2.20.0 (2.20.0). Zenodo. DOI: https://doi.org/10.5281/zenodo.3605514
29. Xu, Z.; Tao, D.; Zhang, Y.; Wu, J.; Tsoi, A.C. Architectural style classification using multinomial latent logistic regression. Fleet, D. et al. (Eds.): ECCV 2014. Available: LNCS 8689 - Architectural Style Classification Using Multinomial Latent Logistic Regression (springer.com)
30. Saputro, D.R.S.; Widyaningsih, P. Limited memory Broyden-Fletcher-Goldfarb-Shanno (L-BFGS) method for the parameter estimation on geographically weighted ordinal logistic regression model (GWOLR). AIP Conference Proceedings 2017. 1868, 040009 (2017); DOI: https://doi.org/10.1063/1.4995124
31. Pavloski, R. Toward sentient neurotechnology: Visual object unity may be structured by and constrain neural interactions. *Proc. of the 3rd Intl. Congress on Neurotechnology, Electronics and Informatics*, pp. 81-90, Nov., 2015. https://www.scitepress.org/papers/2015/55881/55881.pdf
32. Bright, I. M.; Pavloski, R. Hysteresis in the perception of visual unity. *Proc. of the 3rd Intl. Congress on Neurotechnology, Electronics and Informatics*, pp. 49-53, Nov., 2015. https://www.scitepress.org/Papers/2015/56633/56633.pdf
33. Pavloski, R.; Lamb, C. Simulations support the simple hypothesis that persistent coupling of electrochemical activity in recurrent network neurons is an objective signature of visual object unity. *Int. Joint Conf. on Neural Networks*, Anchorage, Alaska, USA, May 14-19, 2017.
34. Rule, M.; Stoffregen, M.; Ermentrout, B. A model for the origin and properties of flicker-induced geometric phosphenes, *PLoS Comput. Biol.*, 7, **2011**, DOI: 10.1371/journal.pcbi.1002158
35. Pavloski, R. Progress in Developing a Neuromorphic Device that is Predicted to Enhance Cortical Prosthetic Vision by Enabling the Formation of Multiple Visual Geometries. U.S. Provisional Patent Application No. 63/354,959, June 23, 2022.